JOURNAL OF CATALYSIS 41, 108–123 (1976)

Catalytic Oxidation of Aqueous Mn(II)

ROBERT W. COUGHLIN AND IWAO MATSUI

Department of Chemical Engineering, Lehigh University, Bethlehem, Pennsylvania 18015

Received March 4, 1975

The oxidation of manganous ion, whether during the formation of nodules in natural waters and undesirable precipitates in water supplies or during processes for removing Mn from potable water, can be catalyzed by a variety of metal–oxide surfaces. The reaction is also autocatalytic because solid manganese oxides catalyze the oxidation. Various solid surfaces possess quite different activities for catalyzing this oxidation and the activity of such catalysts is not simply correlated with tendency to sorb Mn(II). Experimental results are presented for the autocatalytic reaction, for the heterogeneous oxidation reaction and for the sorption of Mn(II) on various solid materials. It is shown that there are wide differences in the catalytic and sorptive behavior of these materials and the results are fitted to simple kinetic models.

INTRODUCTION

The oxidation of divalent, aqueous manganese is of interest for a variety of reasons. From the practical standpoint, this reaction is responsible for the formation of undesirable dark precipitates in water supplies, moreover this unwanted reaction itself can also be harnessed as a catalytic means of removing the Mn from water supplies thereby preventing the formation of such unwanted precipitates. The oxidation of Mn(II) is also of general interest as related, perhaps closely related, to the formation of the deep-sea nodules which abound on the floors of the worlds oceans and fresh water lakes. As is well known plans are now underway to harvest this vast mineral resource. Yet another practical relevance of Mn oxidation is its connection with the operation of MnO_2 electrodes which become irreversible and cannot be reoxidized if they are reduced beyond a certain extent. From the fundamental standpoint this reaction is of interest because the mechanism is so complex, because so little is known about the nature of the active sites and because the overall reaction is autocatalytic: the various solid oxides which are formed as reaction products serve to catalyze the reaction.

METHODS

Background

It has been generally observed that Mn(II) will neither precipitate from aqueous solution nor be oxidized until the pH is raised to about 8 and our observations during the experiments described herein are in accord with such previous observations. In the absence of oxygen the precipitate is at first almost white but darkens rapidly with age; in the presence of oxygen the precipitate is dark brown to black. The pH required for complete oxidation has been reported as 10.3 by Nordell (*1*) and 8.5 by Hem (*2*). Oxidation is accompanied by the liberation of protons which tends to lower pH and reduce the oxidation rate. Morgan and Stumm (*3*) have reported that the rate of oxidation is second order in $[OH^-]$, first order in $[O_2]$ and first order in $[M_n^{2+}]$. Both Hem and Morgan observed the auto-

TABLE 1

Eh–pH Relations for Mn–H_2O System

Equilibrium reaction	Eh–pH
$3M^{2+} + 4H_2O = Mn_3O_4 + 8H^+ + 2e^-$	Eh = 1.824 − 0.237pH − 0.08874 loga (Mn^{2+})
$Mn_3O_4 + 2H_2O = 3MnOOH^a + H^+ + e^-$	Eh = 0.767 − 0.05916pH
$Mn^{2+} + 2H_2O = MnOOH^a + 3H^+ + e^-$	Eh = 1.468 − 0.17748pH − 0.059161 loga (Mn^{2+})
$MnOOH^a = MnO_2 + H^+ + e^-$	Eh = 0.978 − 0.05916pH
$Mn^{2+} + 2H_2O = MnO_2 + 4H^+ + 2e^-$	Eh = 1.225 − 0.11832pH − 0.02958 loga (Mn^{2+})
$3Mn(OH)_2 = Mn_3O_4 + 2H_2O + 2H^+ + 2e^-$	Eh = 0.466 − 0.05916pH
$Mn(OH)_2 + 2H^+ = Mn^{2+} + 2H_2O$	pH = 7.72 − 0.5 loga (Mn^{2+})
$3MnOH^+ + H_2O = Mn_3O_4 + 5H + 2e^-$	Eh = 0.881 − 0.1479pH − 0.08874 loga ($MnOH^+$)
$2Mn^{2+} + 3H_2O = Mn_2O_3 + 6H^+ + 2e^-$	Eh = 1.496 − 0.17748pH − 0.059161 loga (Mn^{2+})
$Mn(OH)_2 + H^+ = MnOH^+ + H_2O$	pH = 4.6902 − loga ($MnOH^+$)
$MnOH^+ + H^+ = Mn^{2+} + H_2O$	pH = 4.6232 − loga (Mn^{2+}) + loga ($MnOH^+$)
$2H_2O = O_2 + 4H^+ + 4e^-$	Eh = 1.229 + 0.01479 log P_{O_2} − 0.05916pH
For reference	
$H_2O_2 = O_2 + 2H^+ + 2e^-$	Eh = 0.682 + 0.002958 log P_{O_2} − 0.05916pH − 0.02958 loga (H_2O_2)
$\frac{1}{2}Cl_2 + H_2O = HClO + H^+ + e^-$	Eh = 1.63 + 0.05916 loga (HClO) − 0.05916pH −0.02958 loga P_{Cl_2}

[a] MnOOH is listed as $Mn_2O_3 \cdot H_2O$ (74).

catalytic effect due to the catalytic action of the precipitated oxides which are products of the reaction.

As the pH of a solution of Mn(II) is increased we expect protons to be lost from the hydrated manganous ions:

$$[Mn(H_2O)_x]^{2+} \rightarrow [Mn(H_2O)_{x-y}(OH)_y]^{(2-y)+} + yH^+.$$

As the charge on the ions is lowered, polymerization of these complex ions may take place. If other cations are present they may well become incorporated into the polymeric ions; if oxygen is present in solution, presumably it would also react with and become incorporated into these complex polymeric ions which are then the precursers of the precipitates of manganese oxides which form upon oxidation at higher pH. At lower pH the stability of the divalent ions may be viewed as due to their high charge which provides the repulsive

TABLE 2

Analysis of Mn^{3+} in Various Manganese Oxides

Sample	Relative amount of Mn(III)–triethanolamine, absorbance
Wet Mn ppt No. 1 obtained at pH 9–10	0.31
No. 2 obtained at pH 10–11	0.35
Dried Mn ppt. No. 1 obtained at pH 10–11 passed through 325 mesh	0.25
β-MnO_2 passed through 325 mesh	0.027
Mn nodule No. 1 passed through 325 mesh	0.95
No. 2 passed through 325 mesh	0.34
No. 3 passed through 325 mesh	0.103

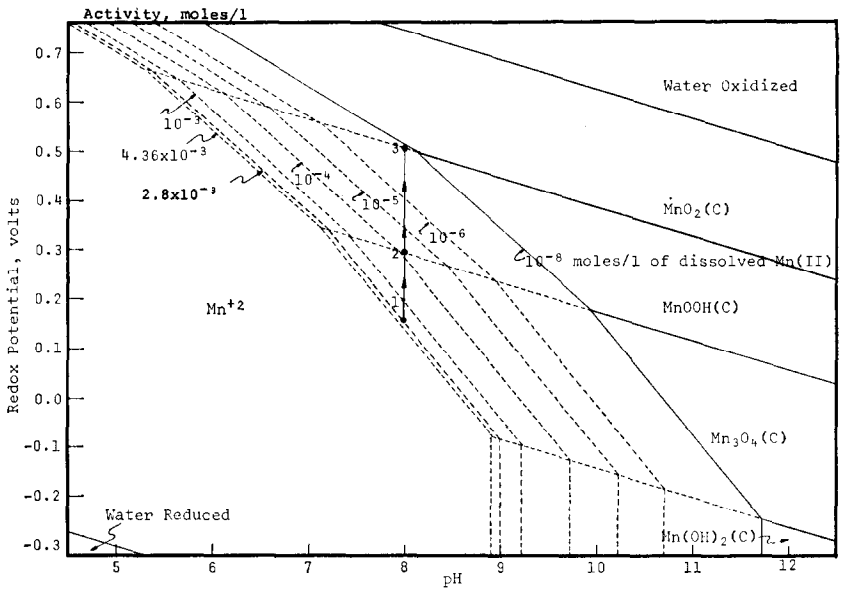

FIG. 1. Stability diagram for MnO_2–O_2–H_2O.

force necessary to prevent polymerization with attendant incorporation of additional oxygen into the structure.

As might be expected, the oxides of Mn formed as precipitates in this way are usually hydrated and nonstoichiometric. Moreover they are usually negatively charged owing to the protons lost during polymerization and oxidation. It is not unexpected that such negatively charged particles would sorb cations and serve as catalysts for further oxidation, thereby incorporating additional oxygen and Mn into the structure.

There are certain well-known stoichiometric oxides of Mn for which chemical

TABLE 3

ANALYSIS OF PRECIPITATED MANGANESE OXIDES[a]

pH at which the Mn precipitated were obtained	Dried sample treated at 180°C for 1 hr		Wet sample	
	Method: potentiometric titration with potassium permanganate			
	Mn precipitated oxides (%)	x^b in MnO_x	Composition (%)	x^b in MnO_x
10	64.5	1.88		
9.5	66.2	1.74	85 Mn_2O_3 15 MnO_2	1.58
9.0	58.1	2.45	30 Mn_2O_3 70 MnO_2	1.84
8.5	57.1	2.55	100 MnO_2	2.00

[a] From aqueous solution initially containing 1.8×10^{-3} moles/liter after Hem (2).
[b] Calculated in this study based on the experimental values of Mn analysis listed.

oxidation half-cell reactions can be written describing their formation from aqueous Mn^{2+}. These are shown in Table 1 together with the corresponding thermodynamic free-energy relationship written in the form of a Nernst equation where Eh is the redox potential. These equations are shown plotted in Fig. 1 for 25°C and atmospheric oxygen pressure. This diagram shows the Eh–pH domains of stability of the various oxides of Mn in the presence of atmospheric oxygen and water. Such diagrams are frequently employed by geochemists to represent such natural phenomena as precipitation and dissolution of minerals. Table 2 shows some experiments carried out on Mn oxides in which 0.5 g of the solid was extracted for 6 months in 15 ml of alkaline, 33% triethanolamine solution. The characteristic green Mn(III) complex formed with triethanolamine (*4*, *5*) was then measured spectroscopically at 534 nm. The presence of Mn(III) is evident, especially in freshly formed precipitates. Table 3 shows the effect of pH of precipitation on the amount of oxygen in the precipitate as well as the fact that drying the precipitate in air promotes further oxidation.

Further evidence for the existence of Mn(III) in the precipitates is provided by Fig. 2 which is a polarogram of a solution resulting from equilibrating a precipitate in 10% triethanolamine in 0.1 *N* KCl. In Fig. 2 the first wave represents the reversible

TABLE 4

SOLID OXIDES AS CATALYSTS

Catalyst	Composition/origin	Mesh size	BET surface area (m^2/g)
α-MnO_2	See below[a]	<325 mesh	34
β-MnO_2	Reagent grade, Baker Chemical Co.	<325 mesh	4
γ-MnO_2	Union Carbide Co.	<325 mesh	78
δ-MnO_2	See below[a]	<325 mesh	100
Mn(II)·manganite	See below[a]	<325 mesh	152
Mn ppt No. 1	Obtained by oxidizing $Mn(NO_3)_2$ in aqueous solution at pH 10–11	<325 mesh	47
$MnO \cdot MnO_2$	Union Carbide Co.		3
Mn nodule No. 1	20°30′N & 114°08′W, 12,000 ft Mn 27.2 wt% Fe 10.8 Ni 1.22 Co 0.13 Cu 0.72 Si 15.2	<325 mesh	190
No. 2	31°54.7′N & 77°25′W, 900 m.	<325 mesh	
No. 3	East side of Santa Cruz Basin off Southern California	<325 mesh	12
No. 4	Phosphate off Coast of Southern California	<325 mesh	
Plagioclase No. 1	$(NaAlSi_3O_8)_{40}(CaAl_2Si_2O_8)_{60}$	<325 mesh	<0.3
Microcline	$KAlSi_3O_8$	<325 mesh	<0.3
Olivine	$(Mg_2SiO_4)_{90-95}(Fe_2SiO_4)_{10-5}$	<325 mesh	1.1
TiO_2 (rutile)	National Lead Co.		160
Fe_2O_3	Baker Chemical Co.		10
Cab-O-Sil (EH-5)	Silica gel/Cabot Corp.	0.001	390 ± 40

[a] Paper by Healey *et al.* [*J. Colloid Interface Sci.* 21, 435 (1966)], outlines procedures for preparing various Mn oxides; these procedures were followed in the present work.

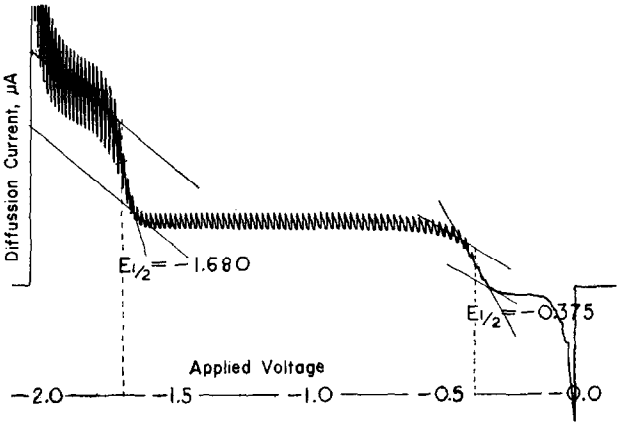

FIG. 2. Polarogram of manganic triethanolamine complex in 0.5 *M* NaOH + 10% triethanolamine + 4.36 m*M* in Mn precipitates + 0.1 *N* KCl.

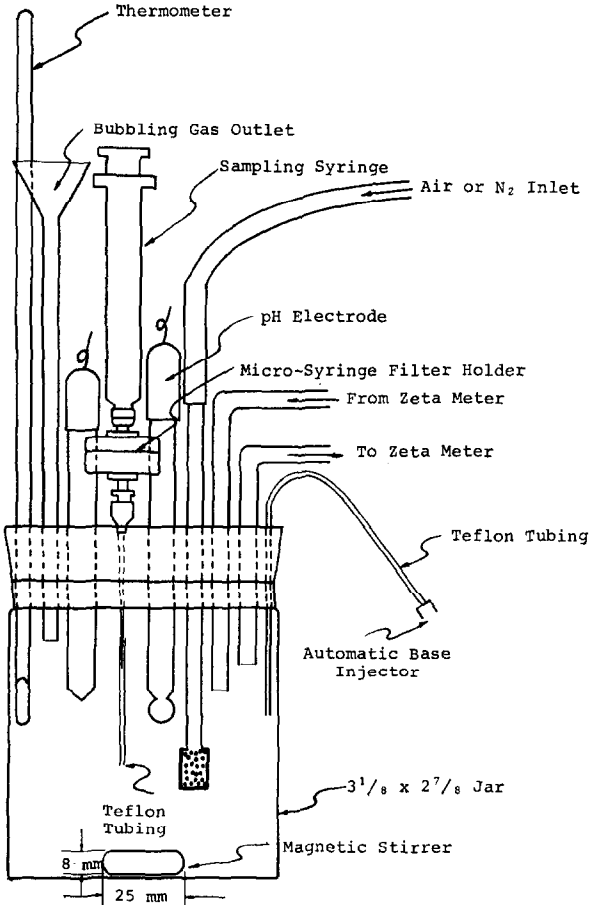

FIG. 3. Manganese reaction cell.

one-electron reduction of the Mn(III)-triethanol complex (half wave potential = − 0.375 V vs SCE) to form the Mn(II) complex; the second wave represents the reduction of the Mn(II) complex to elemental Mn (half wave potential = − 1.685 V vs SCE).

Kinetic Experiments

Figure 3 shows the apparatus used to carry out the experiments. A recorder-controller was used to record pH and maintain the pH set point by automatically injecting base using a syringe drive. Either nitrogen or air could be bubbled through the stirred system (about 200 ml of liquid); when externally added catalysts were studied they were added through the funnel which also served as the gas outlet. The solution was sampled periodically through a Millipore (0.45 μm) filter to exclude particles from the filtered liquid samples ($\sim$1 ml) which were then spectrophotometrically analyzed for Mn(II) using the formaldoxime method (*6*). The conduits indicated in Fig. 3 to and from the Zeta meter were not used in these experiments.

Table 4 describes the various solids (with origin or preparation technique) wich were studied as externally added catalysts for the oxidation reaction and as sorbents for Mn(II) in the absence of oxygen (i.e., while pure N_2 was bubbled through the reaction mixture). In each case 0.20 g of solid was introduced into 200 ml of solution 4.36 m*M* in Mn(II).

Figure 4 shows the course of oxidation at various temperatures in terms of the volume of base vs time. Figure 5 shows the same reactions in terms of the decrease in Mn(II) concentration vs time. One experiment carried out under the same conditions but not shown on these graphs indicated no reaction at pH 7.25 even after 48 hr of bubbling oxygen. The relationship between Mn(II) oxidized and volume of base added is essentially linear up to about 80% of

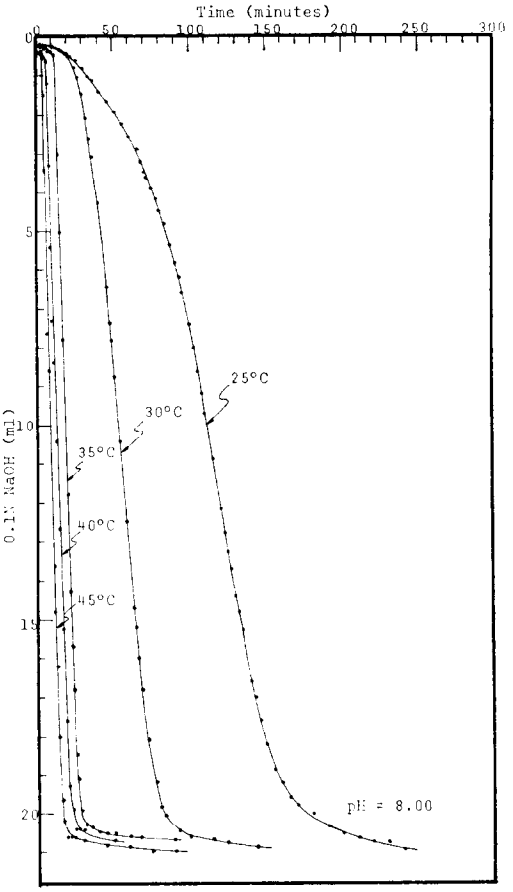

FIG. 4. Rate at which 0.1 *N* NaOH was consumed during the oxidation reaction at various temperatures.

Mn^{2+} oxidized with about 2.8 moles H^+ released per mole Mn^{2+} consumed; near the end of the reaction this relationship decreases from 2.8 to 1.8 moles H^+ per mole Mn^{2+}.

Figure 6 shows the rate as a function of Mn(II) concentration; the shape is typical of autocatalytic reactions. Figure 7 depicts the best curve-fitted values of the rate constants k_1 and k_2 (calculated as explained below) plotted vs reciprocal temperature.

Kinetic Models

Table 5 summarizes several kinetic models which have been employed to fit the

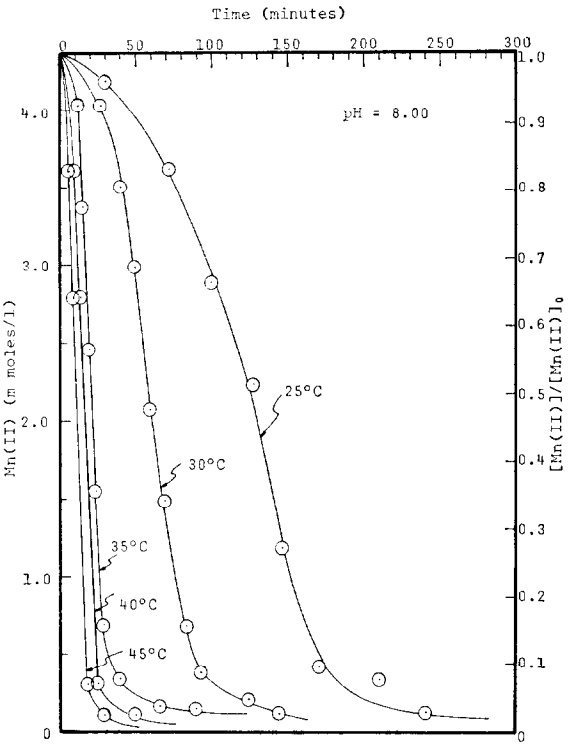

FIG. 5. Oxidation of Mn(II) at various temperatures—with no external catalyst.

experimental data. Model 1 is directed toward the initially homogeneous reaction, without externally added catalyst. This model involves a simple first order (k_1) reaction for the homogeneous formation of solid oxides from aqueous Mn(II) as well as a reaction (k_2) involving the solid manganese oxide thus formed and aqueous Mn(II). Thus the application of Model 1 was carried out by numerically fitting the experimental data over the course of an experiment (see Fig. 8) to the equation:

$$-d[\mathrm{Mn(II)}]/dt = k_1[\mathrm{Mn(II)}] + k_2[\mathrm{Mn(II)}][\mathrm{MnO}_x],$$

with

$$[\mathrm{MnO}_x] = [\mathrm{Mn(II)}]_0 - [\mathrm{Mn(II)}],$$

where the 0 subscript refers to the initial concentration. Model 2 is a simple Langmuir adsorption isotherm describing the sorption of Mn(II) on solid oxides as well as the sorption step of the heterogeneous reactions catalyzed by externally introduced solids as described by:

$$-d[\mathrm{Mn(II)}]/dt = k_3[\mathrm{Mn(II)}]\{[\mathrm{Mn(II)}_s] - [\mathrm{Mn(II)}_a]\} - k_4[\mathrm{Mn(II)}_a],$$

where the subscripts a and s refer, respectively, to surface concentration corresponding to [Mn(II)] in solution and surface concentration corresponding to monolayer coverage. The constants k_3 and k_4 can be evaluated from adsorption experiments in the absence of oxygen.

Models 3 through 5 were used to fit the data obtained with externally introduced catalysts. Model 3 which fits the data for externally added manganese oxide and deep-sea nodule catalysts, is based on fast Langmuir sorption of Mn(II) cations on the solid as in Model 2 followed by slow first-order oxidation of the sorbed species (k_5) with the oxidation rate equal to $k_5[\mathrm{Mn(II)}_a]$. Note that Model 3 incorporates five rate constants: k_1 through k_5.

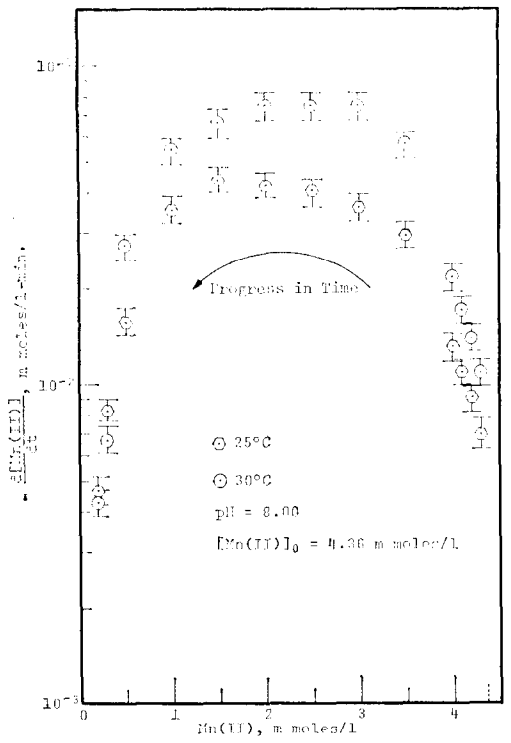

FIG. 6. $-(d[\mathrm{Mn(II)}]/dt)$ vs Mn(II) for Mn(II) oxidation.

Model 4, which provides a good fit of the data for plagioclase and olivine, postulates that the externally introduced solid S′ must itself first be oxidized (k_7) before it will directly sorb and simultaneously oxidize Mn(II) (k_6'). In Model 4 S′ represents sites on the externally added catalyst depleted in oxygen and S_{0x} represents corresponding oxygenated sites active for oxidation of Mn(II). The corresponding rate equation is:

$$-d[\mathrm{Mn(II)}]/dt = k_1[\mathrm{Mn(II)}] + k_2[\mathrm{Mn(II)}][\mathrm{MnO}_x] + k_6[\mathrm{Mn(II)}],$$

with

$$[\mathrm{Mn(II)}]_0 = [\mathrm{Mn(II)}] + [\mathrm{MnO}_x].$$

Implicit in this equation is the assumption that k_7 is very large, thereby permitting the substitution $k_6 = k_6'[S_{0x}]$; i.e., a constant, steady-state concentration of oxygenated sites S_{0x} on the externally added catalyst. Note that both Models 3 and 4 also retain

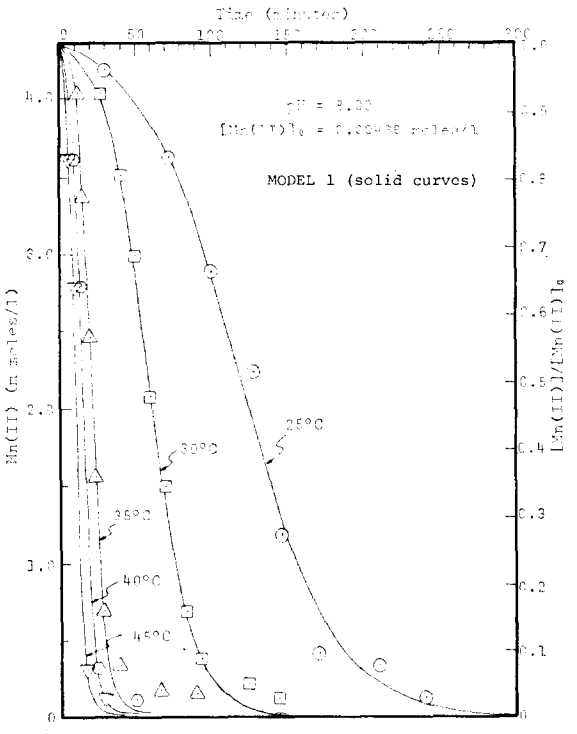

FIG. 7. Test of kinetic model 1 for Mn(II) oxidation at various temperatures.

TABLE 5

COMPARISON OF THE MODELS

Model	Application to chemical reaction
1	Autocatalyzed oxidation of Mn(II) with no externally introduced catalyst. Reaction pattern: $\mathrm{Mn(II)} \xrightarrow[k_1]{O_2} \mathrm{MnO}_x\mathrm{(S)}$ $\mathrm{MnO}_x\mathrm{(S)} + \mathrm{Mn(II)} \xrightarrow[k_2]{O_2} 2\mathrm{MnO}_x\mathrm{(S)}$ (fast)
2	Adsorption of Mn(II) on various solid oxides from deoxygenated solution. Reaction pattern $\mathrm{Mn(II)} + \mathrm{S} \underset{k_4 \text{ desorption}}{\overset{k_3 \text{ adsorption}}{\rightleftharpoons}} \mathrm{Mn(II)\cdot S}$
3-5	Oxidation of Mn(II) in the presence of externally introduced catalyst. Autocatalyzed oxidation (Model 1) is assumed to take place in parallel with reactions catalyzed by external catalyst.
3	External catalyst has active sites which adsorb Mn(II) in preference to oxygen, and subsequently adsorbed Mn(II) is oxidized. Reaction pattern: Model 1 $\mathrm{Mn(II)} + \mathrm{S} \underset{k_4}{\overset{k_3}{\rightleftharpoons}} \mathrm{Mn(II)\cdot S} \xrightarrow[O_2]{k_5} \mathrm{MnO}_x$
4	External catalyst has active sites which adsorb oxygen in preference to Mn(II), and oxygenated sites oxidize Mn(II). Reaction pattern: Model 1 $\mathrm{S'} + \mathrm{O}_2 \xrightarrow{k_7} \mathrm{S}_{0x}$ $\mathrm{S}_{0x} + \mathrm{Mn(II)} \xrightarrow{k_8} \mathrm{MnO}_x + \mathrm{S'}$
5	External catalyst has both active sites for adsorbing Mn(II) and oxygen. Reaction pattern: combination of Models 1, 3 and 4

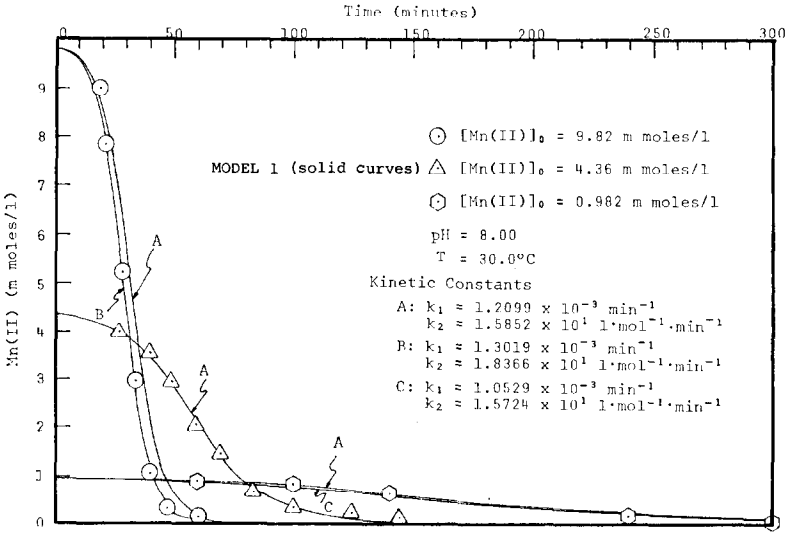

FIG. 8. Test of kinetic Model 1 for concentration dependency of Mn(II) oxidation.

all features of Model 1; i.e., all models allow for the (k_2) oxidation of Mn(II) to be catalyzed by the surface of Mn oxides formed by reaction on the externally introduced catalyst.

Model 5 which provides a good fit for the rutile and Fe_2O_3 catalysts is merely a combination of Models 3 and 4; i.e., it supposes that the reactions of these other models take place simultaneously with the assumption, $k_6 = k_6'[S_{0x}]$, as in Model 4. For a fuller explanation of these kinetic models, the numerical solution of the corresponding differential rate equations and the adjustment of parameters k_1–k_7 in fitting the rate data, the reader is referred to the dissertation of Matsui (*7*) upon which this paper is based.

Figure 7 shows the fit of Model 1 to data obtained at several different temperatures for the initially homogeneous reaction with no externally added catalyst. Figure 8 demonstrates that the goodness of fit is relatively independent of the starting concentration of Mn(II). Figure 9 shows Arrhenius plots for the parameters $k_1(E_A = 26$ kcal/mole) and $k_2(E_A = 34$ kcal/mole for 25–35°C and $E_A = 9$ kcal/mole for 35–45°C). Since a smooth curve, rather than two straight lines, could as easily be described by the data points for the heterogeneous reaction it is possible to surmise a transition from observation of rates of chemical reaction at lower temperatures to observation of rates of diffusion (from solution to particles) at higher temperatures. At lower temperatures the activation energy of the heterogeneous reaction appears to be greater than that of the homogeneous reaction thereby suggesting that the catalyst may provide many additional (active sites) pathways of somewhat greater activation energy rather than only alternative reaction pathways of lower activation energy. This remains only a suggestion, however, because five data points are inadequate to support convincingly any such argument. Figures 10 and 11 show reasonable agreement between Model 2 (Langmuir adsorption) and the data for sorption

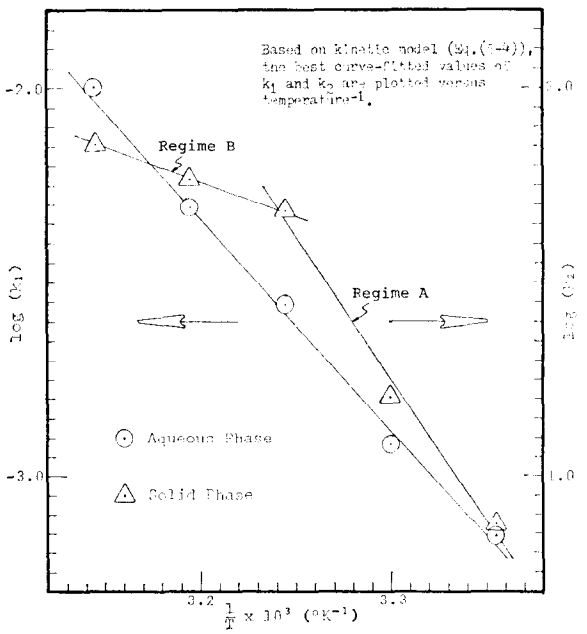

FIG. 9. Arrhenius temperature dependence of the homogeneous and heterogeneous reactions—no externally added catalyst.

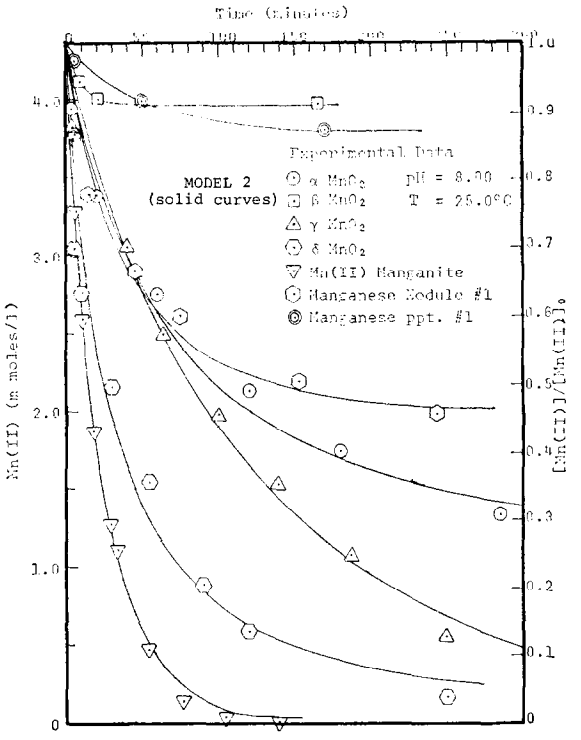

FIG. 10. Test of kinetic Model 2 for adsorption of Mn(II) on various solid oxides. All solutions deoxygenated by bubbling nitrogen.

of divalent Mn on 10 different solid oxides in the absence of oxygen (i.e., in an N_2 atmosphere). It should be stressed that at pH 8 no precipitation occurs.

The predictions of Model 3 are compared to the data obtained with externally added catalytic solid oxides in Figs. 12 and 13. It is seen that the results obtained with 5 manganese oxides and a deep-sea nodule fit Model 3 rather well but the data for silica do not conform to this model so well. Figures 14 and 15 show that Model 3 provides a very poor fit for catalysis by TiO_2 and Fe_2O_3. Figure 16 shows that Model 4 fits the data for plagioclase and olivine rather well. Figure 17 shows that Model 5 predicts reasonably well the reaction as catalyzed by Fe_2O_3 and TiO_2, solids for which neither Models 3 nor 4 provide a good fit. One interpretation might be then that TiO_2 and Fe_2O_3 possess one kind of sites which function for the sorption of Mn(II) and another kind for the sorption of oxygen.

When the observed kinetic rate constants are interpreted together with the measured BET surface areas of the various solids employed as catalysts one computes active site concentrations ranging from about $6 \times 10^{15}/cm^2$ for the most highly oxidized Mn oxides to about $5 \times 10^{14}/cm^2$ for TiO_2 and $2 \times 10^{14}/cm^2$ for the Cab-O-Sil silica.

DISCUSSION

From the kinetic parameters it is possible to estimate the surface concentrations of sites for Mn(II) adsorption. This information is summarized in Table 6 where it is seen that most materials have such sorption site densities in the range of 10^{14}–$10^{15}/cm^2$; here no values of site density appear for plagioclase and olivine since these materials displayed kinetics which did not follow a model based on Mn(II) sorption but rather on oxygen adsorption. No estimate of oxygen-adsorption site density was made but

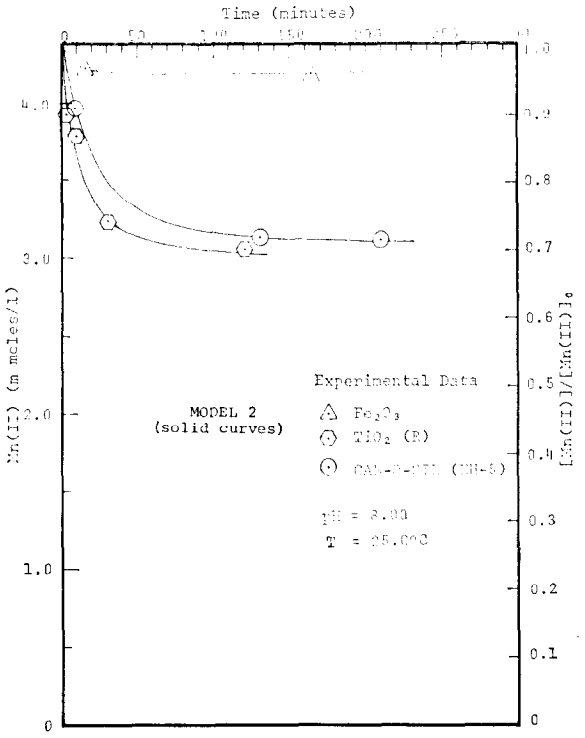

FIG. 11. Test of kinetic Model 2 for adsorption of Mn(II) on various solid oxides. All solutions deoxygenated by bubbling nitrogen.

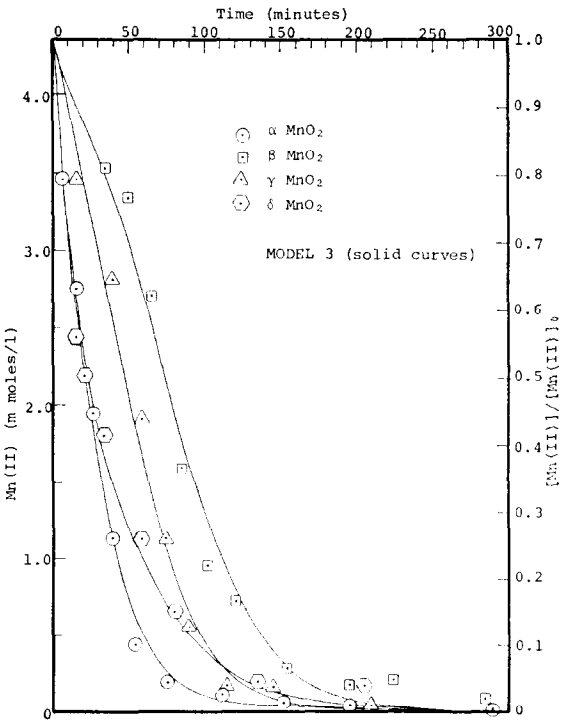

FIG. 12. Test of kinetic Model 3 for heterogeneous oxidation of Mn(II).

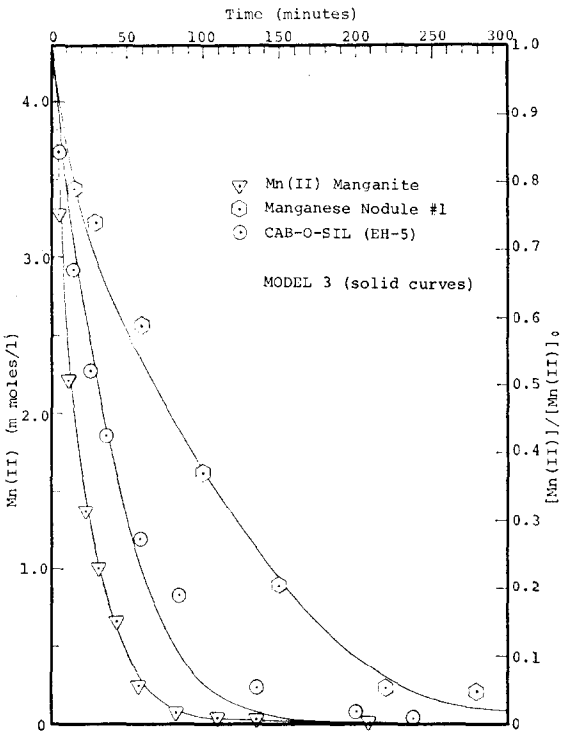

FIG. 13. Test of kinetic Model 3 for heterogeneous oxidation of Mn(II).

it appears that, based on the immeasurably small sorption capacities observed for plagioclase, microcline and olivine for Mn(II) (i.e., less than 0.001 mmoles/g) the oxygen sorption sites on these materials are far sparser than the Mn(II) sorption sites on the other materials.

The results for the sorption of Mn(II) on the other materials in the absence of oxygen show better conformity to Model II in the

TABLE 6

KINETIC CONSTANTS, AND ACTIVE SITES EVALUATED BASED ON PROPOSED KINETIC MODELS[a]

No external catalyst added	k_1 min^{-1}	k_2 (liters $mole^{-1}$ min^{-1})	k_3 (liters $mole^{-1}$ min^{-1})	k_4 (min^{-1})	k_5 (min^{-1})	k_6 (min^{-1})	Active sites (moles/g)	Active sites (No./cm²)
	6.981×10^{-4}	7.305						
External catalysts	Surface area (BET) (m^2/g)							
			3.673	1.817×10^{-4}				
α-MnO_2	34		1.084×10^{1}[b]	2.552×10^{-4}[b]	5×10^{-1}		3.375×10^{-3}	5.976×10^{15}
β-MnO_2	4		2.570×10^{1}	2.939×10^{-5}	3×10^{-1}		3.954×10^{-4}	5.951×10^{15}
γ-MnO_2	78		9.764×10^{-1}	3.191×10^{-6}	5×10^{-2}		9.944×10^{-3}	7.675×10^{15}
δ-MnO_2	100		8.062	3.817×10^{-6}	5×10^{-3}		4.789×10^{-3}	3.882×10^{15}
Mn(II)·manganite	152		4.801	1.586×10^{-5}	1×10^{-2}		1.103×10^{-2}	4.370×10^{15}
Mn ppt	47		5.123	3.933×10^{-6}			5.878×10^{-4}	7.529×10^{14}
Mn nodule No. 1	190		7.076	2.06×10^{-9}	1×10^{-3}		2.347×10^{-3}	7.438×10^{14}
Cab-O-Sil (EH-5)	390 ± 40		9.446	2.06×10^{-9}	1×10^{-1}		1.258×10^{-3}	1.942×10^{14}
Olivine	1.1					6.501×10^{-4}		
Plagioclase	<0.3					1.457×10^{-4}		
TiO_2 (R)	160		1.9001×10^{1}	2.742×10^{-5}	2	0.015	1.289×10^{-3}	4.849×10^{14}
Fe_2O_3	10		3.604×10^{1}	4.379×10^{-6}	2×10^{-2}	0.004	1.664×10^{-4}	1.002×10^{15}

[a] $[Mn(II)]_0 = 0.00346$ moles/liter, catalyst = 1.0000 g/liter of a sample, at 25°C and pH = 8.0.
[b] Evaluated from the data of the initial stage of the adsorption reaction.

later stages than in the earlier stages where the measured sorption rates were higher. This behavior may be explained on the basis of flocculation of the fine particles in the early stages (which was visually observed) whereafter the sorption rate in the later stages could be retarded by diffusion into the floccules.

Based on the results it may be concluded that the autocatalytic oxidation of Mn(II) arises from the attendant formation of solid catalytic oxidation products having surface areas as high as 47 m^2/g. The reaction is accompanied by the release of H^+. The ratio of H^+ released to Mn(II) oxidized is about 2.8 up to the stage at which about 80% Mn(II) is oxidized and then decreases to about half this value near the end of the reaction. This behavior is reflected in the formation of nonstoichiometric oxides of Mn. Indeed, the reactions are very complex (far more complex than suggested by the simplified models employed above) and yield mixed products having different oxidation states because adsorption and oxidation take place simultaneously on the surfaces of incipiently formed oxides. The detected presence of Mn(III), with more of this ion in the freshly precipitated oxides than after they are dried in air, suggests that Mn(III) ions exist in the precipitated oxides in metastable form. Furthermore the observed presence of Mn(III) in deep-sea nodules suggests that the oxidation mechanism of Mn(II) in natural waters may involve Mn(III) as an intermediate.

When Mn(II) is adsorbed from deoxygenated solution, the ratio of H^+ released to Mn(II) adsorbed ranges between 2.1 and 2.2 for the various solids during most of the course of sorption, except for the earliest stages where the ratio is lower. The sorption of polyvalent metal ions is a complex process because not only OH sites, but also sorbed H_2O, may interact with metal ions. Since much more H^+ is released from the solids in the presence of Mn(II) it is believed that OH sites are not present on the

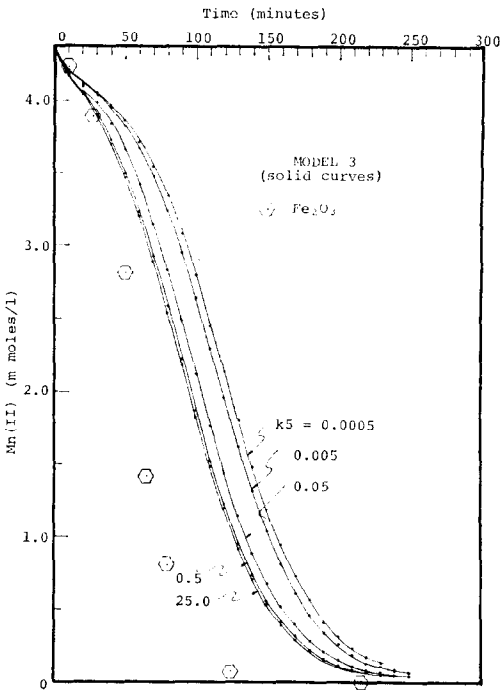

FIG. 15. Kinetic Model 3 as applied to oxidation of Mn(II) on Fe_2O_3.

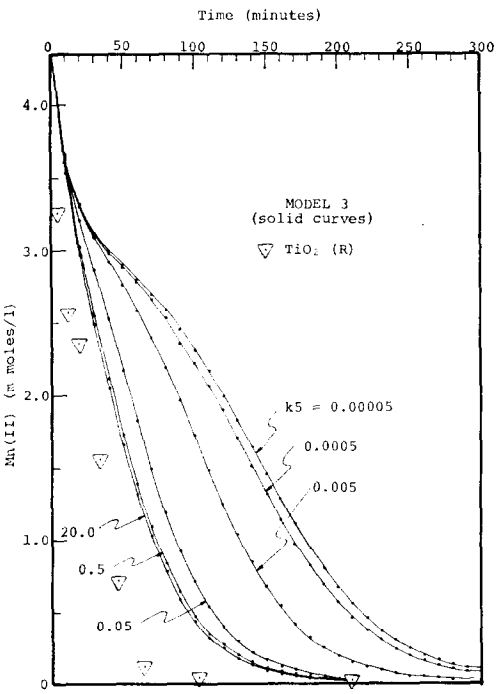

FIG. 14. Kinetic Model 3 as applied to oxidation of Mn(II) on TiO_2.

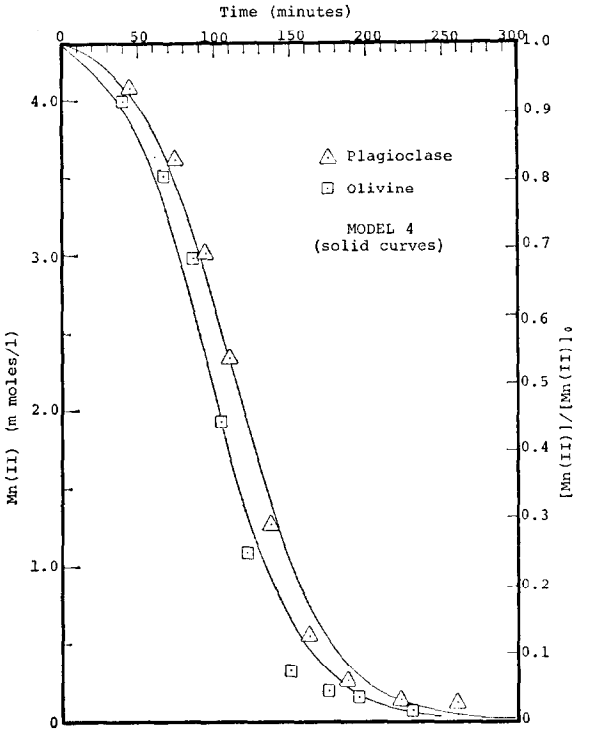

FIG. 16. Test of kinetic Model 4 for heterogeneous oxidation of Mn(II).

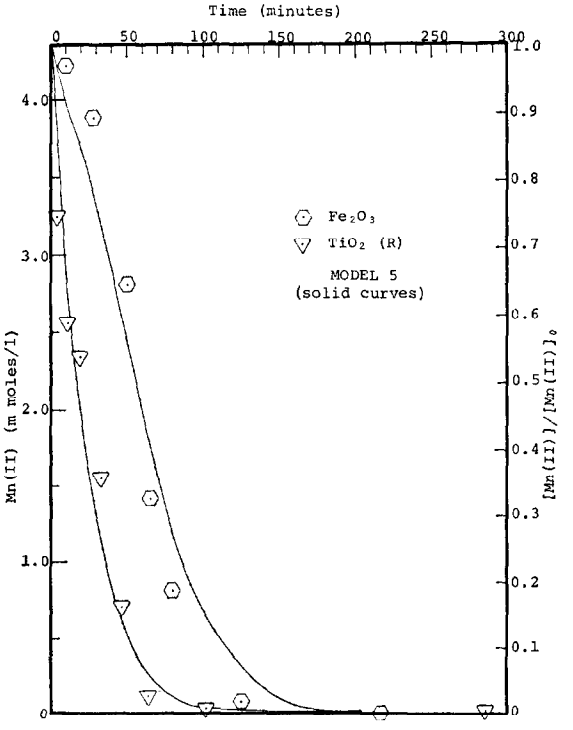

FIG. 17. Test of kinetic Model 5 for heterogeneous oxidation of Mn(II).

surface initially in concentrations sufficient to account for all the Mn(II) sorbed. Fast sorption of Mn(II) at OH sites may underlie the lower ratio of H^+ released to Mn(II) sorbed in the early stages; an alternative explanation could involve the incorporation of Mn(II) into disordered lattices of the various materials, especially the Mn oxides.

ACKNOWLEDGMENTS

The authors are grateful to the National Science Foundation for support under Grant GA-825, to Mobil Oil Corp. and the William C. Gottshall Fellowship fund for additional financial support, and to Dr. William Snyder for helpful discussion and assistance with experiments.

REFERENCES

1. Nordell, E., *Water Sewage Works* **11**, 181 (1953).
2. Hem, J. D., *U. S. Geol. Surv. Water Supply Pap.* 1667A (1963).
3. Morgan, J. J., and W. Stumm, *Proc. Int. Water Pollut. Res. Conf. 2nd* p. 103 (1965).
4. Asaoka, H., *Jap. Anal.* **12**, 1144 (1963).
5. Perisi, R., *Ann. Chim. (Rome)* **44**, p. 59 (1954).
6. Snell, F. D., and C. T. Snell, "Colorimetric Methods of Analysis," Vol. 2, pp. 395–396 Van Nostrand, New York, 1954.
7. Matsui, I., PhD dissertation, Leigh Univ., 1973.